DOI: 10.13009/EUCASS2019-214

Characterization of miniature Hall thruster plume in the 50 - 200 W power range

S. Mazouffre[1†], T. Hallouin[1,2], M. Inchingolo[1], A. Gurciullo[2], P. Lascombes[2], J.-L. Maria[2]

[1] CNRS, ICARE laboratory, Orléans, France

[2] Exotrail, Massy, France

[†] Corresponding author; stephane.mazouffre@cnrs-orleans.fr

Abstract

After a brief introduction to micropropulsion devices for small spacecraft and low-power Hall thruster performances in terms of thrust and specific impulse, this study focuses on plasma plume properties. The plume of the 100 W-class ISCT100-v2 Hall thruster has been characterized with two types of electrostatic probes. The ion current was measured with a Faraday cup while the ion energy was determined using a 4-grid RPA. Angular distributions of ion current density and ion EDF recorded in the plume far-field for several thruster parameters are presented and commented. Besides, direct thrust measurements performed with a micro-balance are compared to thrust values inferred from plume data.

1. Introduction

Over the last decade, spacecraft miniaturization has opened up a new space market with great potential. Technologically simple, inexpensive and flexible, nano- and micro-satellites (1 – 200 kg) offer numerous possibilities for LEO missions when used in constellation. Propulsion systems naturally has to adapt to the new requirements through miniaturization and power consumption reduction. Due to limitations in terms of volume and mass, electric thrusters are better suited for very small satellites compared to their chemical counterpart. In fact, the high specific impulse (Isp) of electric propulsion devices directly translates into a low propellant amount for a given mission profile. There are various types of small low-power electric thruster technologies according to the way thrust and Isp are produced [1-4]. The thruster collection covers a very broad range of operating parameters, therefore most micro-satellite mission needs can be satisfied when selecting the proper device. Among all technologies, Hall thrusters currently offer the highest thrust density (~ 60 mN/kW) and thrust-to-power ratio (> 20 N/m^2) with an Isp above 1000 s [1,5]. Moreover, the recently validated magnetically shielded configuration opens up the way to total impulse in excess of 500 MNs, making achievable ambitious interplanetary missions, see [6] and references herein. Although the Hall thruster technology in the 1 – 10 kW range is mature and safe, miniaturization and low-power operation are still challenging on efficiency and lifetime viewpoints. The size reduction that is necessary to maintain a sufficient ionization rate in the plasma discharge leads to the increase in plasma/surface interactions, which in turn negatively impacts thrust production and component wear [7].

In this contribution we present performances and characteristics of miniature Hall thrusters operating below 300 W input power. After a comparison of various EP devices and a short description of typical performances of low-power Hall thrusters, this work focuses on plasma plume characterization in terms of ion current and ion energy. Plume studies are essential for miniature Hall thruster optimization for three reasons. Firstly, plume data reflects the physics at play in the plasma discharge and thruster near field. Secondly, ion flow properties are directly linked to performance parameters and figures of merit. Thirdly, plume data is needed for the validation of plume/spacecraft numerical simulation outcomes. The accurate prediction of plasma plume interactions with spacecraft elements is critical from a mission objective standpoint as ion impacts can damage elements of the spacecraft like solar arrays and differential charging between various parts may lead to electrical arc formation [8-10]. In addition, measurements in EP device plumes are required for development and optimization of efficient and reliable diagnostic instruments for the purpose of ion beam diagnosis standardization as requested by space agencies.

All experiments have been performed in the NExET vacuum chamber with a 100 W-class permanent magnet Hall thruster. The device has been fired with xenon as propellant over a broad range of discharge voltages and mass flow rates. The ion current density and the ion energy in the plasma plume have been measured by means of a Faraday cup and a repulsing potential analyzer, respectively. The thrust, from which the efficiency and the Isp can been inferred, has been measured using a recently-developed mN-range thrust balance. Angular profiles of ion current density and

DOI: 10.13009/EUCASS2019-214

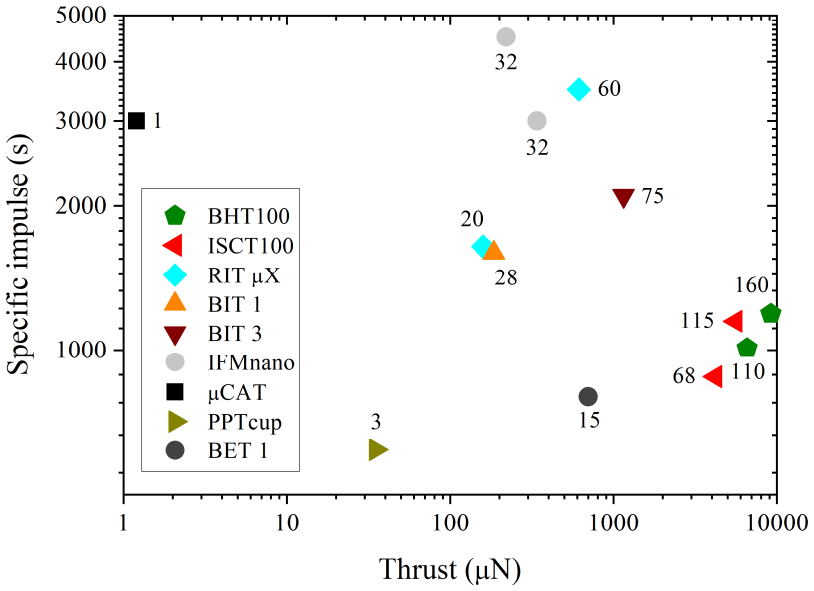

Figure 1: Specific impulse against thrust for various types of electrical microthrusters: Hall thruster (BHT100, ISCT100), Gridded ion engine (RIT μX, BIT 1 and 3), FEEP (IFM nano), VAT (μCAT), PPT (PPTcup) and electrospray thruster (BET 1). Numbers in the graph indicate the input electrical power.

ion energy distribution function acquired far downstream the HT exit plane for several operating conditions are presented and discussed in this contribution. Quantities like total ion current, current utilization, propellant utilization and beam voltage are also shown and their evolution with thruster parameters is reported and commented. Finally, the thrust level computed from a combination of total ion current and mean ion energy is compared to the one directly obtained with the micro-balance.

2. Low-power EP device performances

2.1 Comparison between various microthruster types

Figure 1 shows the specific impulse versus thrust level map for several types of electrical microthrusters, namely Vacuum arc thrusters (VAT), Pulsed plasma thrusters (PPT), Field Emission electric propulsion (FEEP) devices, electrospray thrusters, gridded ion engines and Hall thrusters [2-4]. VAT and PPT use solid-state propellant. FEEP and electrospray thrusters operate with liquid propellant. GIE and HT use gaseous propellant, typically xenon. All thrusters described in Figure 1 require less than 200 W input power.

As can be seen in Figure 1, propulsion systems can be divided into two main categories: high Isp devices versus low Isp devices, setting arbitrarily the boundary at 2000 s. PPT, electrospray thruster and Hall thrusters belong to the second group. Hall thrusters are, however, characterized by a thrust-to-power ratio and a thrust density larger than the ones achieved by other low Isp devices. Moreover, for a given power, high Isp devices necessarily produce a low thrust level due to energy conservation law [1].

2.2 Comparison between various Hall thrusters

Figures 2a and 2b show the thrust and the specific impulse as a function of the input power, respectively, for 7 different low-power Hall thrusters. More information about the thrusters and related publications can be found in [11]. In figure 2a, the thrust varies linearly with the power in the 50 – 300 W range from 5 mN to about 20 mN. The specific impulse also increases from 600 s to approximately 1600 s as indicated in Figure 2b. In general high thrust – low Isp operation of a HT is achieved with a large propellant mass flow rate and a relatively low (around 250 V) discharge voltage. The anode efficiency of low power HTs typically increases from 0.2 to 0.45 in the range of interest, see [11].

DOI: 10.13009/EUCASS2019-214

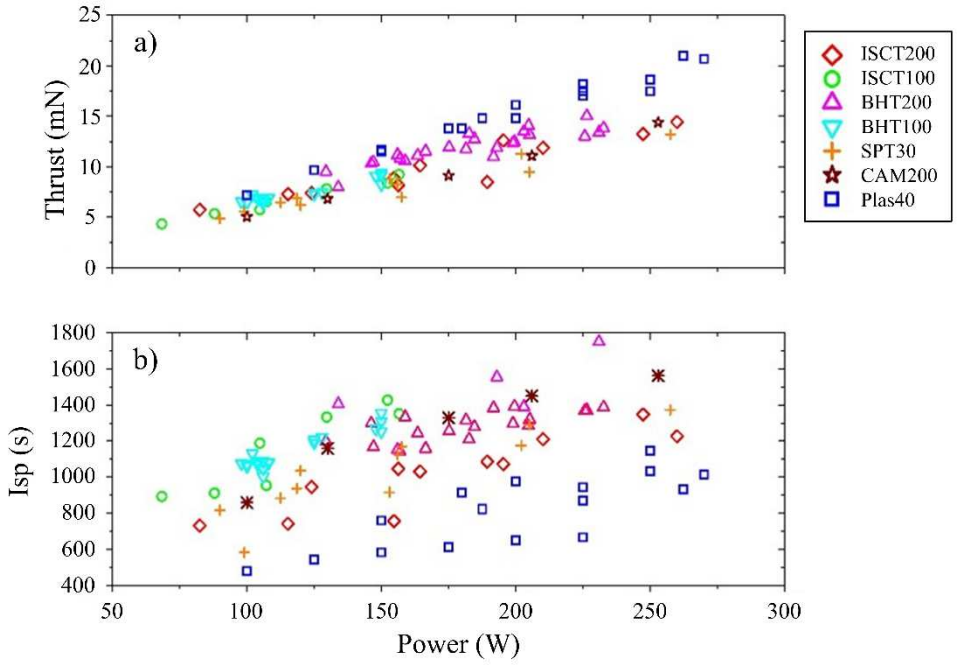

Figure 2: a) Thrust as a function of power and b) specific impulse as a function of power for 7 different low power Hall thrusters fired with xenon [11].

At 150 W input power, a Hall thruster fuelled with xenon and equipped with BN or BN-SiO_2 channel walls usually generates about 10 mN of thrust with a specific impulse around 1000 s and an anode efficiency around 30 - 40 %. The thrust-to-power ratio therefore reaches ~ 65 mN/kW.

3. Experimental arrangement

3.1 Vacuum chamber – Hall thruster

All experiments have been performed in the cryogenically pumped NExET (New Experiments on Electric Thrusters) vacuum chamber, a stainless steel tank 1.8 m in length and 0.8 m in diameter. Primary pumping is provided by a dry pump that evacuates 400 m^3/h. A 350 l/s turbomolecular pump further pumps the chamber down to 10^{-6} mbar-N_2, by absorbing water vapours and light gases such as N_2, O_2 and H_2. The cryogenic pump absorbs gases such as xenon and krypton. The pumping speed is around 8000 l/s when the 0.5 m^2 cold panel is sustained at 35 K. The overall pump stack guarantees a background pressure as low as 2×10^{-5} mbar-Xe during operation of a 400 W input power plasma source. A large water-cooled screen covered with graphite tiles is mounted at the rear of the chamber to absorb part of the ion beam energy, thereby reducing the thermal load on the cryogenic surface. The chamber is equipped with several observation windows, access ports and vacuum feed-through connectors for power lines, gas lines and diagnostic tools. A large front door enables easy access to the interior of the vessel.

The 100-W-class ISCT100-v2 Hall thruster has been used in these studies [12]. The annular channel was in the $2S_0$ geometrical configurations, where S_0 corresponds to the channel cross-sectional area of the well-known Russian SPT100 thruster. Walls were made of BN-SiO_2 ceramic. The magnetic field is generated by way of small cylindrical samarium– cobalt (SmCo) magnets brought together inside rings located on either side of the channel walls. A soft iron magnetic circuit with a back gap permits to shape the desired topology. No magnetic screen is used. The magnetic field has a classical bell-shape distribution along the channel centerline with the highest intensity at the channel exit plane. The magnetic field maximum magnitude was $2B_0 = 2 \times B_0$ here [12]. The propellant gas is injected homogeneously inside the channel using a high porosity mullite ring placed behind the channel back plate. A narrow annular gap in the back plate allows diffusion of the gas. The anode is a wide stainless steel ring placed at the back of the channel against the internal surface of the outer dielectric wall. During operation, the thruster body was floating. A 1 A-class heated LaB_6 hollow cathode was used to generate the electron current needed for discharge balance and

DOI: 10.13009/EUCASS2019-214

ion beam neutralization. The cathode was located outside the channel with its orifice in the vertical plane that contains the channel outlet. The cathode was electrically connected to the thruster anode and floating.

Discharge envelope and current oscillation level of the ISCT100-v2 thruster can be found in reference [12] for a broad range of powers and various configurations. During these experiments, the xenon mass flow rate injected in the channel was varied from 5 to 7 sccm and the applied voltage was ramped up from 200 to 350 V. The discharge current therefore varied between 0.35 and 0.65 A and the input power stayed in the 50 – 200 W range.

3.2 Plume diagnostic tools

Faraday cup

A Faraday Cup (FC) is a special kind of electrostatic planar probe; It is basically an isolated conductive cup dedicated to the detection of charged particles in a low-pressure or vacuum environment [13,14]. When a Faraday cup operates as an ion collector, which means the cup is negatively biased with respect to the floating potential, the ion current in the probe direction can be accurately measured. Contrary to a planar probe, edge effects due to plasma sheath formation are negligible with a FC. Besides a FC limits flow and plasma perturbations (local pressure increase, shock wave, contamination), secondary electron emission has a relatively weak impact upon measurement outcomes and the probability for ion capture is high.

In this study, a Faraday cup with a 10 mm in diameter graphite collimator has been used. The collimator is electrically insulated from the cup using a PEEK ring [13]. The FC is encapsulated into a cylindrical aluminum pod to be protected from fast ion bombardment. During measurements the pod is floating with respect to the local plasma potential. The pod is also used to mount the probe onto its holder. A grounded 2410 *Keithley* sourcemeter instrument is used for simultaneously polarizing the FC and measuring the collected ion current.

Repulsing potential analyser

A Retarding Potential Analyzer (RPA), also known as Retarding Field Electrostatic Analyzer (RFEA), is a gridded probe that uses electric fields to act as an energy filter [15-17]. An efficient RPA design contains 4 grids and a collector, as shown in Figure 3.
- The first grid at the entrance of the probe serves to shield the plasma from the field inside the probe in order to minimize plasma disturbance. The grid is often either at floating potential or grounded although setting the grid at the local plasma potential is the most efficiency approach.
- The second grid is negatively polarized with respect to the plasma potential. It permits to repel electrons hence ensuring only ions enter the instrument.
- The third grid is an ion repeller. This grid has a variable positive potential applied to it. By adjusting the potential one can scan the ion energy distribution. Ions with energies below the grid potential are repelled and prevented from being detected.
- A fourth grid is often added behind the ion repeller, which is biased negative to prevent secondary electrons emitted by the current collector from escaping. Note that the potential of G4 is below the potential of G2 not to trap electrons inside the device (hence to limit ionization of the residual gas).
- The ion collector can be biased negative to act as an ion collector (useful when the ion energy is very low) or it can be grounded.

In a RPA, the grid mesh size as well as the gap between grids must be optimized to ensure a proper electric field configuration to guide ions towards the collector. The mesh size is of a few Debye lengths and the gap is typically ~1 mm. Grids are typically made of carbon or Mo. The grid mount must be built to avoid short-circuits due to grid material sputtering and subsequent conducting-coating formation. The first two-grids are especially concerned. Naturally, the ion collector is made of a low SEE yield material like Mo or W. A collimator placed ahead the first grid can be used to limit the ion flux and to better select the ion entry angle. When possible, the RPA must be evacuated by a pump to limit the residual gas pressure, therefore decreasing the number of charge exchange collision events inside the device. The entire RPA must be protected against ion bombardment with e. g. the use of graphite shields.

A RPA acts as a high-pass filter: only ions with voltages, that is energy-to-charge ratios, greater than the repeller grid voltage can pass and reach the collection electrode. The potential of the ion retarding grid is then varied while monitoring the ion current incident on the collector; thus data are obtained as current versus voltage. The negative derivative of the $I(V)$ trace is then directly proportional to the ion energy distribution function (IEDF) [15,17].

DOI: 10.13009/EUCASS2019-214

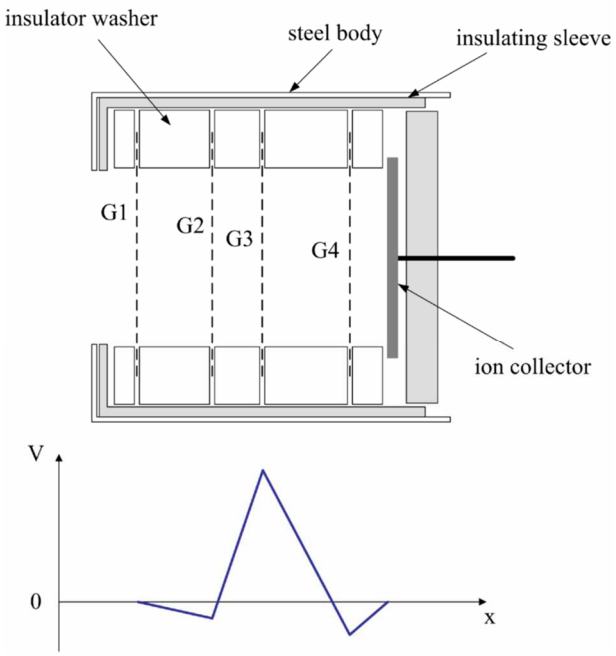

Figure 3: 4-grid RPA schematic: shielding grid (G1; floating, grounded or V_p), electron repelling (G2; $V < 0$), ion retarding (G3; V variable), secondary electron suppression (G4; $V < 0$). Also shown is the potential structure within the probe with a grounded current collector (0 refers to ground).

As a RPA is an electrostatic device, it cannot distinguish between singly charged and multiply charged ions. The current measured by a RPA is not dependent on the ion energy, but rather on the energy per unit charge of the ion species. Thus a singly-charged ion with 300 eV of energy and a doubly-charged ion of 300 eV of energy will be filtered identically by the probe.

The 4-grid RPA used in this work has the following characteristics. The entrance orifice was 10 mm in diameter. Grids were in stainless steel, with 0.4 mm in diameter holes and a 60 % transparency. G1 was floating, G2 was set at -15 V, G3 voltage was swept between 0 and 400 V and G4 was fixed at -20 V. The collector was made of Mo and grounded. The Semion control unit from *Impedans Ltd* has been used to power the RPA and acquire the *I-V* curves.

The Faraday cup and the RPA were installed on a rotating arm in aluminum of which the pivot point lies in the vertical plane that contains the thruster channel exit and is aligned with the thruster centerline. The two measuring instrument axis is in the horizontal plane that includes the thruster axis. The distance between the HT exit plane and the instrument entrance orifice is here 31.5 cm, that is about 10 thruster diameters. Rotation of the arm is controlled by means of a URS100BCC motorized rotation stage from *Newport*. The rotation angle θ is varied between -90° and +90°, the thruster axis corresponding to $\theta = 0°$.

4. Plasma plume properties

4.1 Ion current density

The angular distribution of the ion current density j_i measured in the plasma plume of the ISCT100-v2 thruster firing at 200 V with 5 sccm xenon is shown in Figure 4 for two values of the FC bias voltage, namely -25 V and -75 V. The two distributions are similar that indicates the plasma sheath expansion has no impact upon the measured current as expected with a FC geometry [13]. In the rest of this paper the probe was biased at -70 V.

As can be seen in Figure 4, the current density profiles are symmetrical with respect to the thruster axis. The on-axis magnitude is around 0.25 mA/cm^2 not far from what is usually found for higher power devices (~ 1 mA/cm^2) at the

DOI: 10.13009/EUCASS2019-214

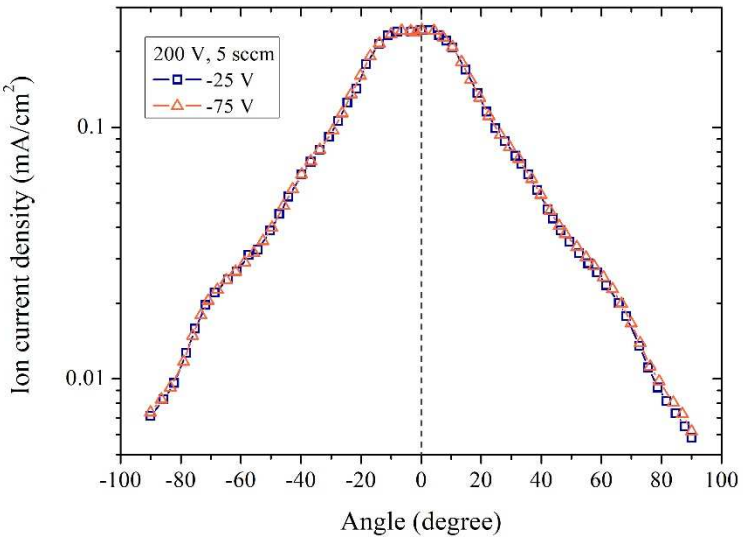

Figure 4: Angular profile of the ion current density in the beam of the ISCT100-v2 Hall thruster for two different bias voltage of the Faraday cup (200 V, 5 sccm, I_d = 0.38 A, 3×10^{-5} mbar).

nominal operating point. The on-axis value of j_i appears to be relatively invariant for optimized HTs, i.e. not much influenced by the power level and the size [5]. The current density sharply decreases when mowing away from the thruster axis. There are about two orders of magnitude difference in j_i between 0° and ±90°. A slight increase in j_i is observed around ±60° in Figure 4. This special feature has also been noticed with high power Hall thrusters [13].

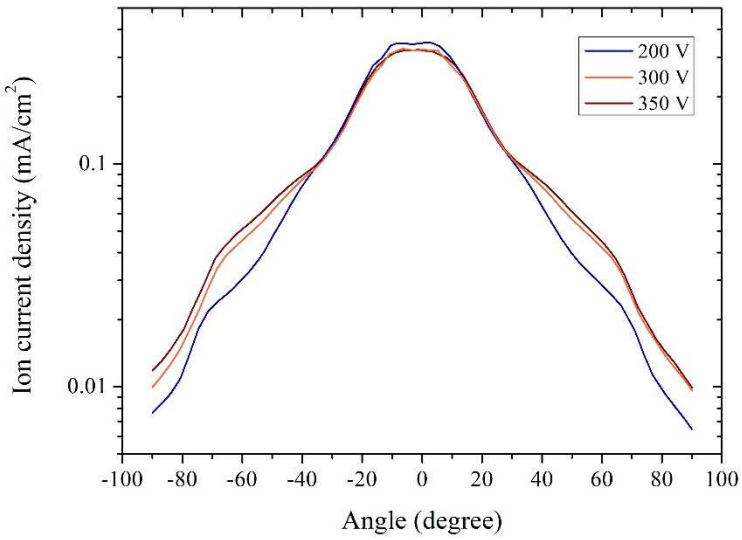

Figure 5: Angular profile of the ion current density in the beam of the ISCT100-v2 Hall thruster for three discharge voltages (6 sccm, 5×10^{-5} mbar).

DOI: 10.13009/EUCASS2019-214

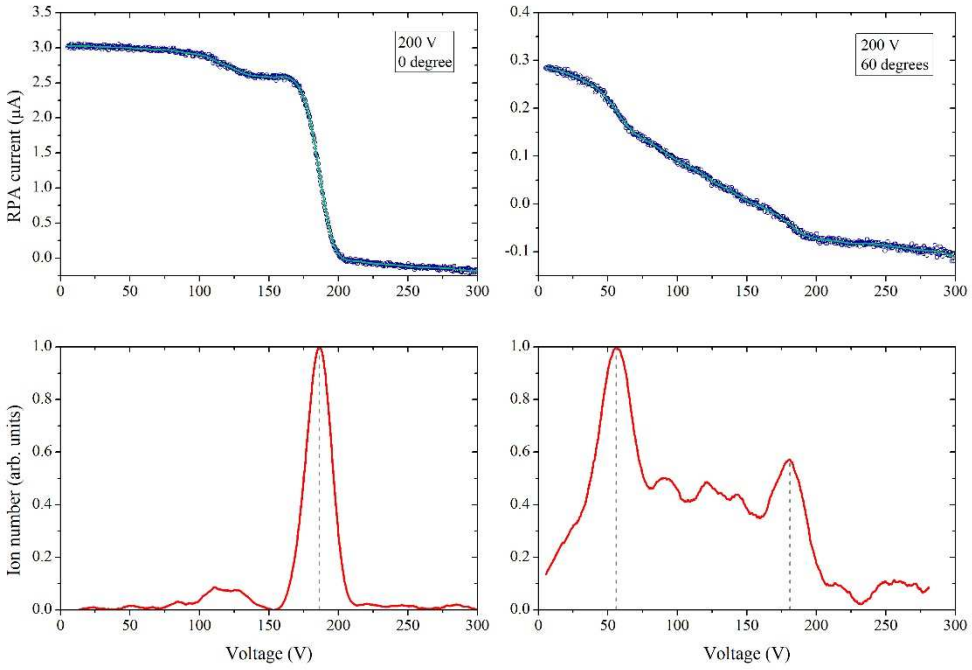

Figure 6: RPA current-voltage trace at 0° (left) and 60° (right). Also shown is the corresponding ion EDF (bottom). Operating conditions of the ISCT100-v2 Hall thruster: 200 V, 5 sccm, 3×10^{-5} mbar.

Figure 5 illustrates the influence of the thruster discharge voltage on the ion current density angular distribution. The core of the beam, i.e. the region in the vicinity of the thruster axis, does not change when the voltage is varied. Defining the core as the unaffected region, this one thus spreads from 0° to ±30° here. The highest value of j_i is around 0.4 mA/cm^2.

The ion current density increases in the wing, $\theta >$ ±30°, when the applied voltage is ramped up as shown in Figure 5. As the background pressure remains unchanged at 5×10^{-5} mbar changes in the angular profile shape cannot be attributed directly to the residual gas. Several explanations are possible at this point. Firstly, the number of charge-exchange and diffusion collision events could increase with the voltage as the ion kinetic energy increases. Secondly, the fraction of multiply-charged ion species increases with the voltage, such ions being predominantly scattered at large angles [18]. Finally, more ions, whatever their electrical charge, could be scattered at large angles due to a change in the electric field topology and/or in the location of the ionization zone in the channel. Additional measurements, eg with an E×B probe, as well as computer simulations are needed to understand and explain the observed phenomenon.

4.2 Ion energy

Energy distribution function

Examples of current-voltage traces measured with the RPA in the plume of the ISCT100-v2 thruster are given in Figure 6. The I-V curves have been recorded with identical operating conditions (200 V, 5 sccm) but at two different angles. The corresponding ion Energy Distribution Function (EDF) are also shown in Figure 6.

It is obvious that the angle has a drastic impact on the ion EDF. The distribution measured on the jet centreline reveals a main peak with a mean energy of 186 eV close to the discharge voltage, the gap corresponding to the cathode reference potential (CRP). The width (FWHM) of the dominant peak is about 20 eV, which gives an idea about the energy spread in the ionization region. A secondary small peak is visible around 120 eV. It probably contains ions that have experienced collisions nearby the channel outlet where the atom density is still large. Notice the small peak is quite broad with a width around 40 eV, which is in agreement with a collision event process.

The ion EDF measured at 60° shows a complicated shape with many peaks, see Figure 6. The dominant peak is at 52 eV that means the plume is dominated by slow ions at large angles. Those ions result from charge-exchange and

DOI: 10.13009/EUCASS2019-214

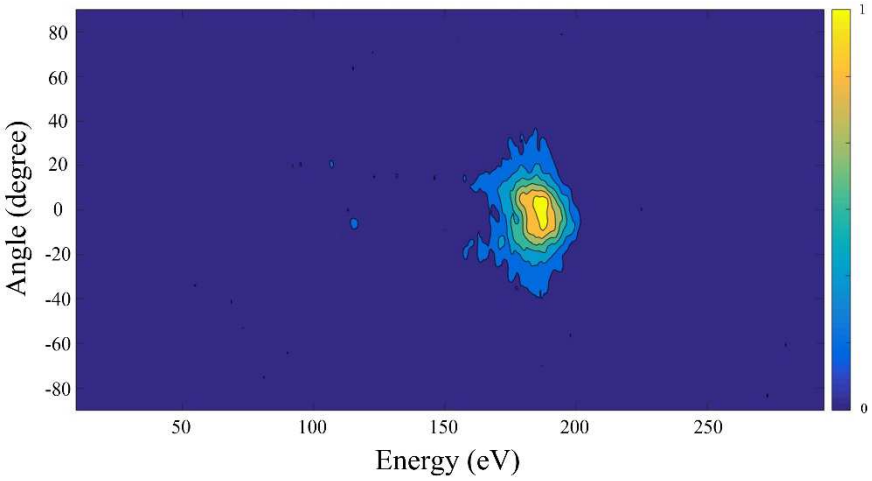

Figure 7: Contour plot of the normalized ion EDF as a function of the angle (200 V, 5 sccm).

scattering collisions. The peak that corresponds to ions that have experienced the entire potential drop in the acceleration zone is at 180 eV, which indicates energy losses. A large part of the ion EDF contains ions with energies between 50 and 180 eV. Ion EDFs displayed in Figures 6 highlight the complicated Hall thruster plume structure in terms of energies, especially at large angles [18-20]. They also reveal the existence of 3 main ion groups: ions from the unperturbed beam, ions scattered at the channel outlet and ions that have experienced collision events in the plume near field and far field.

Figure 7 is a contour plot of the ion EDF as a function of the angle when the ISCT100-v2 operates at 200 V discharge voltage and 5 sccm xenon mass flow rate. Although ions with low velocities flow at large angles, the associated density, or current, is relatively low. As can be seen in Figure 7, a large fraction of ions flow within a narrow angle domain ($\theta \in$ = [-30° – +30°] here) with a kinetic energy that approaches the potential energy provided to the thruster.

Most probable and mean energy

The ion mean energy is computed from the 1st order moment of the ion EDF. The most probable energy is simply the energy associated to the largest signal (the maximum of the ion EDF). Figure 8 shows the angular profile of the most probable and the mean ion energies calculated from RPA traces measured at 200 V and 5 sccm. The two profiles are symmetrical with regards to the thruster axis. The mean energy is the highest at $\theta = 0°$ as the beam is not disturbed on the thruster axis. It decreases almost regularly when the angle is changed from 0° to ±90° due to the increasing population of slow ions as previously shown.
The distribution of the most probable velocity as a function of the angle is unexpected. The velocity stays constant around 180 eV from 0° to ±60°, meaning this section of the plume is governed by the fast ion population. The velocity suddenly collapses to about 60 eV and then decreases gradually to 30 eV at ±90°. The discontinuity in the most probable velocity angular distribution may reveal the jet radial boundary. It is worth noticing the angular profile of the ion current density is also modified at the same location, see Figures 4 and 5.

4.3 Ion current – Efficiencies

Using a spherical coordinate system and assuming the plasma plume is axisymmetric about the thruster centerline, the total ion current I_i reads

$$I_i = \pi r^2 \int_{-\pi/2}^{\pi/2} j_i(\theta) \sin(\theta) d\theta \,, \qquad (1)$$

where r is the distance between the channel outlet and the FC orifice. The beam is assumed to be solely composed of singly-charged ions in equation (1). The propellant mass utilization η_m can be determined from the total ion current using the following equation

DOI: 10.13009/EUCASS2019-214

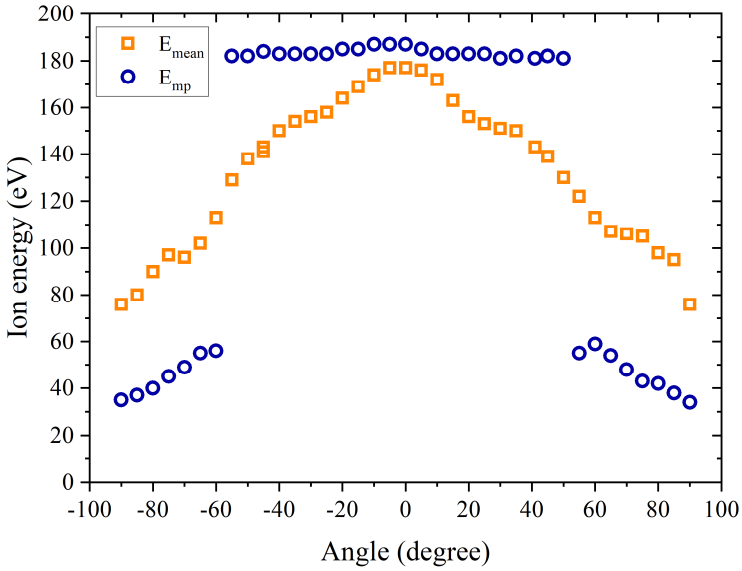

Figure 8: Angular distribution of the ion mean energy (square) and ion most probable energy (circle) at 200 V applied voltage and 5 sccm mass flow rate.

$$\eta_m = \frac{\dot{m}_i}{\dot{m}_a} = \frac{mI_i}{e\dot{m}_a}, \tag{2}$$

where $\dot{m}_a$ and $\dot{m}_i$ are the anode mass flow rate and the ion mass flow rate in the beam, respectively, m is the atomic mass and e is the elementary charge. The total ion current and the ion mean energy in the beam, termed E_{beam}, are displayed in Table 1 for several thruster operating conditions in terms of xenon flow rate and discharge voltage. Several efficiencies are also shown in Table 1 like the current utilization (I_i/I_d), the propellant utilization η_m and the beam voltage utilization (E_{beam}/U_d). The current utilization is above 0.7 on average and the propellant utilization is above 0.8 which demonstrate a good ionization efficiency of the ISCT100-v2 Hall thruster despite a small size and a low input power. The voltage utilization is around 0.7, which shows an efficient energy conversion of the EP system.

The propellant utilization and the voltage utilization both increase when the discharge voltage increases at a fixed mass flow rate. The propellant utilization increases when the mass flow rate increases at a fixed voltage whereas the voltage utilization drops. The current utilization seems to increase with the mass flow rate. It is not much affected by changes in discharge voltages.

Table 1: Discharge current, total ion current, beam energy and efficiencies for several thruster operating conditions.

Thruster parameters			**Plume data**				
U_d	m_a	I_d	I_i	**Current utilization**	**Propellant utilization**	E_{beam}	**Voltage utilization**
V	sccm	A	A	#	#	eV	#
200	5	0.38	0.28	0.73	0.78	144	0.72
300	5	0.46	0.32	0.69	0.88	199	0.7
200	6	0.49	0.35	0.72	0.81	140	0.66
300	6	0.57	0.39	0.68	0.90	205	0.68
350	6	0.58	0.41	0.70	0.95	244	0.7
200	7	0.55	0.43	0.79	0.85	129	0.64
300	7	0.63	0.48	0.75	0.94	214	0.71

DOI: 10.13009/EUCASS2019-214

Table 2: Thrust measured with a thrust stand and inferred from plume data for several thruster operating conditions.

Thruster parameters		Balance		FC - RPA	
U_d	m_a	I_d	*Thrust*	I_d	*Thrust*
V	sccm	A	mN	A	mN
200	5	0.34	**3.8**	0.38	**4.2**
300	5	0.42	**4.8**	0.46	**5.8**
200	6	0.45	**4.6**	0.49	**5.5**
300	6	0.56	**6.5**	0.57	**7.1**
350	6	0.55	**7.3**	0.58	**8.0**
200	7	0.54	**5.7**	0.55	**6.8**
300	7	0.65	**7.9**	0.63	**8.7**

4.4 Thrust level

The thrust can be inferred from plume data using the formula

$$T = \pi r^2 \frac{m}{e} \int_{-\pi/2}^{\pi/2} v(\theta)\cos(\theta) j_i(\theta)\sin(\theta) d\theta \,, \tag{3}$$

where v is the ion velocity determined from the measured ion kinetic energy and the term $\cos(\theta)$ accounts for symmetry in the radial momentum. Thrust value obtained from FC and RPA measurements are given in Table 2 for 7 thruster operating conditions. The thrust level increases with the applied voltage and with the xenon mass flow rate.

The thrust has also been directly measured with a recently developed micro-balance [21,22] presently able to measure forces from 200 μN to about 30 mN with thrusters of several 100s g. The thrust stand can be accommodated into the NExET vacuum chamber. The balance is a counterbalanced-type pendulum. The moving part is fixed to an aluminum U-shape frame by means of two flexural pivots. The thruster is mounted on the bottom section of the pendulum arm whereas an adjustable counterweight is mounted on the upper part to increase the sensitivity. Vibrations and oscillations of the pendulum are damped by means of an eddy current brake. Displacement of the pendulum arm due to an applied force is measured with both a magnetic sensor and a laser-based optical system for redundancy and cross-checking purposes. Measuring devices are calibrated in situ to account for thermal drift with known masses loaded onto a short arm attached to the rotating section. The measurement error is estimated to be around ±200 μN with the current design.

Outcomes of direct thrust measurements are summarized in Table 2. The agreement between the direct and the indirect methods is rather as can be seen. The two estimations agree within 20 % and the two methods give identical tendencies for the evolution of the thrust with the mass flow rate and the discharge voltage. The indirect approach that relies on FC and RPA measurements however always give larger thrust values.

5. Conclusion

Ion current density and ion energy have been measured in the far-field plume of the low-power ISCT100-v2 Hall thruster by means of a Faraday cup and a 4-grid RPA in the [50 – 200] W power range. The propellant utilization is found to be above 0.8 for all operating conditions despite the small thruster size and the low input power. The RPA study reveals the plume contains slow ions with kinetic energies far below the applied potential, at large angles in particular. However, the beam is mostly composed of fast ions confined in a relatively narrow angular domain. On the thruster axis the beam energy approaches the applied potential, the gap being the CRP.

DOI: 10.13009/EUCASS2019-214

Direct thrust measurements carried out with a microbalance have been compared to outcomes of an indirect approach that relies on quantities obtained with the FC and the RPA. The two methods are in relatively good agreement, which shows plume data can be used i) to verify thrust stand data and ii) to assess thruster performances.

Complementary plume measurements will be performed with a 200 W-class Hall thruster to further investigate the influence of size and power on plasma plume properties. In addition, E×B measurements will be carried out in the plume far-field to determine the fraction of multiply-charged ions therefore allowing for a better estimate of current and mass efficiencies and performances.

Acknowledgements

This work has been performed in the frame of the ORACLE joint-laboratory. It was also financially supported by the Région Centre-Val de Loire through the PEPSO-2 program. T. Hallouin benefits from an Exotrail PhD grant.

References

[1] S. Mazouffre, 2016, Electric propulsion for satellites and spacecraft: established technologies and novel approaches, *Plasma Sources Sci. Technol.* 25, 033002.

[2] I. Levchenko et al, 2018, Space micropropulsion systems for Cubesats and small satellites: From proximate targets to furthermost frontiers, *Appl. Phys. Rev.* 5, 011104.

[3] W. P. Wright, P. Ferrer, 2015, Electric micropropulsion systems, *Progress in Aerospace Sciences* 74, 48–61.

[4] D. Krejci, P. Lozano, 2018, Space propulsion technology for small spacecraft, *Proceedings of the IEEE* 106, 362–378.

[5] J-P. Bœuf, 2017, Physics and modeling of Hall thrusters, *J. Appl. Phys.* 121, 011101.

[6] L. Grimaud, S. Mazouffre, 2018, Performance comparison between standard and magnetically shielded 200W Hall thrusters with BN-SiO2 and graphite channel walls, *Vacuum* 155, 514–523.

[7] K. Dannenmayer, S. Mazouffre, 2011, Elementary scaling relations for Hall effect thrusters, *J. Propulsion Power* 27, 236–245.

[8] D. M. Goebel and I. Katz, 2008, Fundamentals of Electric Propulsion, John Wiley & Sons, Inc., New York.

[9] H. B. Garrett, 1981, The charging of spacecraft surfaces, *Reviews of Geophysics* 19, 577–616.

[10] I.D. Boyd, A. Ketsdever, 2001, Interactions between spacecraft and thruster plumes, *J. Spacecraft Rockets* 38, 380–380.

[11] L. Grimaud, S. Mazouffre, 2018, Performance comparison between standard and magnetically shielded 200 W Hall thrusters with BN-SiO_2 and graphite channel walls, *Vacuum* 155, 514–523.

[12] S. Mazouffre, L. Grimaud, 2018, Characteristics and performances of a 100 W Hall thruster for Microspacecraft, *IEEE Trans. Plasma Sci.* 46, 330–337.

[13] S. Mazouffre et al, 2017, Evaluation of various probe designs for measuring the ion current density in a Hall thruster plume, Proceedings of the 35th International Electric Propulsion Conference, Atlanta, Ga, IEPC paper 2017-336.

[14] D. L. Brown et al, 2017, Recommended practice for use of Faraday probes in electric propulsion testing, *J. Propul. Power* 33, 582– 613.

[15] C. Böhm, J. Perrrin, 1993, Retarding-field analyzer for measurements of ion energy distributions and secondary electron emission coefficients in low-pressure radio frequency discharges, *Rev. Sci. Instrum.* 64, 31–44.

[16] S. D. Johnson, M. M. El-Gomati, L. Enloe, 2003, High-resolution retarding field analyzer, *J. Vac. Sci. Technol. B* 21, 350–353.

[17] K. M. Lemmer, A. D. Gallimore, T. B. Smith, D. R. Austin, 2007, Review of two RPAs for use in high density Helicon plasma, Proceedings of the 30th International Electric Propulsion Conference, Florence, Italy, IEPC paper 2007-161.

DOI: 10.13009/EUCASS2019-214

[18] L. B. King, A. D. Gallimore, C. M. Marrese, 1998, Transport-property measurements in the plume of an SPT-100 Hall thruster, *J. Propul. Power* 14, 327.

[19] C. M. Marrese, A. D. Gallimore, J. Haas, J. E. Foster, L. B. King, S. W. Kim, 1995, An investigation of stationary plasma thruster performance with krypton propellant, Proceedings of the 31st Joint Propulsion Conference, San Diego, California, AIAA paper 95-2932.

[20] B. E. Beal, A. D. Gallimore, 2003, Energy analysis of a Hall thruster cluster, Proceedings of the 29th International Electric Propulsion Conference, Toulouse, France, IEPC paper 03-035.

[21] J. E. Polk, A. Pancotti, T. Haag, S. King, M. Walker, 2013, Recommended Practices in Thrust Measurements, Proceedings of the 33rd International Electric Propulsion Conference, Washington, DC, IEPC paper 2013-440.

[22] F. Trezzolani et al, 2017, Development of a counterbalanced pendulum thrust stand for electric propulsion, Proceedings of the 4th IEEE International Workshop on Metrology for AeroSpace, Padua, Italy, 152–157.